PROCEEDINGS OF SPIE

SPIEDigitalLibrary.org/conference-proceedings-of-spie

Hard x-ray characterization of a HEFT single-reflection prototype

Finn Erland Christensen, William W. Craig, Charles J. Hailey, Mario A. Jimenez-Garate, David L. Windt, et al.

Finn Erland Christensen, William W. Craig, Charles J. Hailey, Mario A. Jimenez-Garate, David L. Windt, Fiona A. Harrison, Peter H. Mao, Eric Ziegler, Veijo Honkimaki, Manuel Sanchez del Rio, Andreas K. Freund, M. Ohler, "Hard x-ray characterization of a HEFT single-reflection prototype," Proc. SPIE 4012, X-Ray Optics, Instruments, and Missions III, (18 July 2000); doi: 10.1117/12.391602

SPIE.

Event: Astronomical Telescopes and Instrumentation, 2000, Munich, Germany

Hard X-ray characterization of a HEFT single reflection prototype

Finn E. Christensen[a]
William W. Craig[b], Charles J. Hailey[b], Mario A. Jimenez-Garate, David L.Windt[b]
Fiona A. Harrison[c], Peter H. Mao[c]
Eric Ziegler[d], Veijo Honkimaki[d], Manuel S. Del Rio[d], Andreas K. Freund[d]
Michael Ohler[e]

[a]Danish Space Research Institute, Juliane Maries Vej 30
2100 Copenhagen, Denmark
[b]Columbia Astrophysics Lab, Columbia University, 136 So. Broadway
Irvington, NY 10533, USA
[c]Caltech, 1201 E. California Blvd, MC 220-47
Pasadena, Ca, 91125, USA
[d]European Synchrotron Radiation Facility, B.P.200-F
38043 Grenoble CEDEX, France
[e]IMM, Institute of Microtechnology, Carl Zeiss Strasse 18-20
Mainz, D-55129, Germany

ABSTRACT

We have measured the hard X-ray reflectivity and imaging performance from depth graded W/Si multilayer coated mirror segments mounted in a single reflection cylindrical prototype for the hard X-ray telescopes to be flown on the High Energy Focusing Telescope(HEFT) balloon mission. Data have been obtained in the energy range from 18 - 170 keV at the European Synchrotron Radiation Facility and at the Danish Space Research Institute at 8 keV. The modeling of the reflectivity data demonstrate that the multilayer structure can be well described by the intended power law distribution of the bilayer thicknesses optimized for the telescope performance and we find that all the data is consistent with an interfacial width of 4.5 Å. We have also demonstrated that the required 5% uniformity of the coatings is obtained over the mirror surface and we have shown that it is feasible to use similar W/Si coatings for much higher energies than the nominal energy range of HEFT leading the way for designing Gamma-ray telescopes for future astronomical applications. Finally we have demonstrated 35 arcsecond Half Power Diameter imaging performance of the one bounce prototype throughout the energy range of the HEFT telescopes.

Keywords: Hard X-ray optics, Multilayers, Synchrotron radiation, High Energy Astrophysics

1. INTRODUCTION

Present generation astronomical focusing X-ray telescopes have been limited in energy bandwidth by the fact that the maximum angle of grazing incidence for which significant reflection can be achieved with traditional metal coatings is roughly inversely proportional to the energy. This has limitied the bandwidth of current focusing X-ray telescopes to be below 10 keV because at some point it becomes impractical to achieve significant area for telescopes of reasonable focal lenghts and, in addition the field of view of the instrument becomes undesirably small. Astronomical imaging in the hard X-ray band and the gamma-ray band has traditionally been done using either coded masks or collimators. The approximate equality of the collecting and the detector areas of this type of instrument severely limits the faint source sensitivity as internal detector background rates dominate typical source fluxes in this band. It is, however, possible to extend the graze angle at which significant reflectivity can be obtained in focusing X-ray telescopes by replacing the traditional metal coating with a depth graded multilayer coating.[1,2] X-ray multilayers

Further author information: (Send correspondence to Finn E. Christensen)
Finn E. Christensen: E-mail: finn@dsri.dk

In *X-Ray Optics, Instruments, and Missions III*, Joachim E. Trümper, Bernd Aschenbach, Editors,
Proceedings of SPIE Vol. 4012 (2000) • 0277-786X/00/$15.00

consist of alternating layers of a high electron density element (typically W, Ni or Pt) and a low electron density element(typically Si or C). For a given energy a constant period multilayer will reflect X-rays at angular positions determined by Braggs law. If the period is varied in depth in such a way that soft X-rays(large periods) are Bragg reflected in the top of the stack and the harder X-rays are reflected in the bottom of the stack(small periods) one achieves a structure which can effectively reflect hard X-rays up to 3 times the total external reflection range of the material combination.[3] These so called X-ray supermirrors form the basis for several hard X-ray focusing telescopes which are currently being developed for astronomical applications. Among these are hard X-ray telescopes developed for two balloon payloads, The High Energy Focusing Telescope(HEFT) developed by Caltech, Columbia University and the Danish Space Research Institute(DSRI)[4] and Infocus, being developed by Goddard Space Flight Center and Nagoya University in Japan.[5] In addition NASA's next X-ray observatory, the Constellation-X Mission[6] will incorporate a multilayer coated hard X-ray telescope.[7] The HEFT mission aims at extending the energy bandwidth to 69.5 keV (the W-K absorption edge)using W/Si as the multilayer material combination.[8] Alternative material combinations, are currently being studied to extend the energy bandwidth to higher energies.[8,9] InFocus plans on having the energy cut off at 40-50 keV[10] and the hard X-ray telescope on the Constellation-X mission is likely to extend the energy bandwidth to 100 keV. All of these missions will employ a conical approximation to the Wolter I design. In this paper we describe a hard X-ray reflectivity and imaging study of a single reflection prototype optic based on the novel thermally slumped glass technology developed for the HEFT mission.[11,12] Due to atmospheric absorption the low energy cut off for the HEFT mission is 20 keV.[4] The data presented in this paper was taken at two beamlines(BM5 and ID15A) at ESRF - The European Synchrotron Radiation Facility allowing us to cover the energy range from 18 keV to several hundred keV. In addition data were taken at 8 keV at DSRI. In the next section we give details of the prototype optic and the optimized coatings . This is followed by a section which presents the reflectivity data including coating uniformity measurements of the realistically sized mirror segments and details of the experimental arrangement at ESRF. The subsequent section presents the modeling of the reflectivity data. This is followed by a section giving the imaging characterization and derivation of the one bounce Half Power Diameter(HPD) at both soft and hard X-ray energies and finally a conclusion is presented.

2. SINGLE REFLECTION PROTOTYPE

Once fully instrumented the HEFT payload will consist of 14 coaligned telescope modules with a 6 m focal length. Each module will contain 72 nested mirror shells in a double reflection conical approximation to the Wolter I design. Each mirror shell is divided into a number of segments and each segment is a thermally slumped thin DESAG[11,12] glass substrate coated with a depth graded multilayer. The minimum radius for each telescope module is 4 cm and the maximum radius is 12 cm. In the context of HEFT a systematic method to optimize the design of depth graded multilayers for hard X-ray telescopes[8] has been developed. The method is based on employing a figure of merit which explicitly incorporates the energy bandpass and the field of view for a chosen telescope geometry. The basis for the optimization is a power law distribution of the bilayer thicknesses[3] where the i'th bilayer thickness, d_i , is given by $d_i = a/(b+i)^c$. where a,b and c are constants and i is the i'th bilayer ranging from 1 to N, with i=N being the bilayer next to the substrate. The optimization results in a complete specification of the multilayer coatings by specifying the minimum bilayer thickness $d_{\mathrm{min}} = d_N$, the maximum bilayer thickness $d_{\mathrm{max}} = d_1$, the ratio between the thickness of the heavy element to the bilayer thickness(Γ), the power law index(c) and the number of bilayers(N). Ideally one would optimize the coating for each of the 72 mirror shells. We have, however, found that dividing the 72 mirror shells into 10 groups logarithmically spaced in on-axis angle is a reasonable compromise between complexity in the optimization process and optimal performance. Table 1 gives our current baseline optimization of the HEFT W/Si coatings.[8]

For our first hard X-ray reflectivity and imaging prototype we have chosen to coat and mount 5 mirror segments in a single reflection cylindrical geometry. The 5 mirror segments are denoted D1, D2, D3, D4 and D5 and their radii are 8.3, 8.4, 8.5, 8.6, and 8.7 cm respectively. This is in the middle of the radius range for HEFT. The coating recipes for the mirror segments are given in Table 1. The length of each mirror segment along the cylinder axis is 200 mm as foreseen for HEFT and the thickness of each mirror segment is 0.3 mm. Both DESAG AF45 and D263 was used as the glass substrate.[11] The mirrors on this prototype were segments covering 90° of the azimuthal aperture of a telescope. Each of the mirrors is separated and positioned by five graphite spacers 1 by 1 mm in cross section and running along the entire length of the mirror segments. The spacers were placed 22° apart in azimuth angle. We define the azimuth angle for the central spacer to be the 0-position. The azimuth angles of the spacers are thus -44°, -22°, 0°, +22° and +44° respectively.

The thermal slumping of the glass substrates was developed at Columbia University[11] where slumped glass substrates with an overall figure error near 30 arcsec are routinely made in the radius range relevant for both HEFT and the hard X-ray telescope on Constellation-X.[13] A previous X-ray reflectivity and scattering study of free standing slumped glass substrates has demonstrated that no degradation of the micro roughness due to the slumping is observed and a micro roughness of 2 Å has been measured after slumping.[14]

The slumped glass substrates were coated in a planar magnetron sputtering facility[15] where a coating process has been developed for the depth graded multilayer coatings.[16]

After coating the mirror segments were mounted using a mounting scheme developed by Columbia University . The mounting scheme is described in Hailey et al and in Craig et al.[11–13]

3. REFLECTIVITY MEASUREMENTS

3.1. Experimental details

All the five mirror segments D1 through D5 have been measured at selected energies from 18 keV to 170 keV. The energies selected from beamline BM5 were 18 keV, 28 keV and 34 keV using a detuned double reflection Si(111) monochromator in reflection geometry. At beamline ID15A we selected to work at 65 keV, 80 keV, 90 keV, 100 kev, 115 keV, 158 keV and 170 keV. Here we used a double reflection Si(311) monochromator in Laue geometry. Each data set is reflectivity versus grazing incidence angle at a constant energy. The spectral purity of the beam was typically 10^{-4} in ΔE/E(FWHM). This is small enough that no broadening or smearing of reflectivity features was observed due to the finite energy bandwidth of the beam for the energies listed above. The angular collimation of the beam was determined in each case by the intrinsic rocking curve width of the monochromator reflection and/or by the width of slits placed in front of and behind the monochromator and was typically 0.07 milliradians. The prototype was mounted in a ring which allowed for precise azimuthal rotation of the unit so that each mirror segment could be illuminated at any azimuthal position. Guard slits were placed in front of the prototype unit to allow for variation in the size of the illuminated spot. The reflected beam as well as the normalizing direct beam was measured using a pin diode. At BM5 the synchrotron ring current was used to monitor the decay of the intensity during the measurement. At ID15A we used a separate beam monitoring pin diode in front of the prototype to track the decay of the beam intensity. All data sets were, however, taken in the matter of minutes to an hour so very litte influence of the decay of the beam intensity was noted. The grazing angle was in each case aligned by using the mirror segment itself as a shadow for the beam. We estimate that systematic misalignments of the grazing angle of incidence is less than 0.2 milliradians.

3.2. Reflectivity data

Representative reflectivity data are shown in figures 1 and 2 for mirror segment D3. Error bars are indicated where they are bigger than the data point and the data points have been connected by a line as a guide for the eye. Figure 1 shows the reflectivity at 18 ,28 ,34 ,65 and 170 keV. The data sets have been shifted by a factor of 10 between each data set for clarity. For each data set we give the azimuthal position, ϕ, at which the data were taken. ϕ = 0 is the position of the central spacer as described above. The small values of ϕ used for these data means that all these data sets are comparable from a coating point of view. Data on the uniformity/quality of the coatings as ϕ deviates significantly from 0 is given in the following subsection. Figure 2 shows the same data as well as data at 80 keV and at 115 keV plotted versus the reciprocal lattice vector q=4π sin(θ)/λ, where θ is the grazing angle of incidence and λ is the wavelength. Again the data are shifted by a factor of 10 between each data set for clarity and data points have been connected by a line to guide the eye. The nominal energy range for HEFT is up to the 69.5 keV K-absorption edge in W using our current baseline design. Figure 1 clearly shows that we achieve the high reflectivity required within the on axis angular range as well as away from it(See Table 1). This demonstrates the high quality of the coatings and the robustness of the optimization of the coatings for HEFT as this guarantees significant off axis response of the telescope modules.[8] Figure 2 shows the effect of absorption in the multilayer stack versus energy as X-rays reflected from a bilayer with a given thickness line up at the same reciprocal lattice vector for all energies. As expected the reflectivity curve becomes flatter and the reflectivity at a given q-value increases(provided q is larger than the value corresponding to the total external reflection region and smaller than the value at which the reflectivity drops due to the value of the minimum bilayer thickness) as the energy increases and the absorption decreases. Immediately above the W-K absorption edge the reflectivity suffers dramatically as seen in the 80 keV data but it is also evident that the effect of the absorption edge is nearly gone at 115 keV and that the reflectivity is

completely recovered at 170 keV demonstrating that depth graded W/Si coatings can be deposited which will give high reflectivity up to near 200 keV at graze angles up to 1.3 mrad. This important experimental result as well as other data taken at high energies from specialized multilayer coatings deposited on test flats[9] opens up for the possibility of designing novel gamma-ray telescopes based on depth graded multilayer coatings and reasonable focal lengths.[17]

3.3. Uniformity measurements

It is important that the depth graded multilayer coatings maintain a constancy of the bilayer thicknesses over the entire surface of realistically sized mirror segments. It has been demonstrated for HEFT that one can tolerate a 5% change of the bilayer thicknesses across the mirror surfaces without a significant influence on the throughput and/or field of view of the telescopes.[18] The current baseline design for HEFT is that it will be made up of 60° segments rather than the 90° segments mounted on the current prototype.[13] The 90° segments, however, allowed us to probe the uniformity and quality of the coating up to and beyond the limits of the current HEFT baseline design. Figure 3 shows the measured reflectivity of mirror segment D3 taken at 34 keV for a number of values of the azimuthal position ϕ. The data have been shifted by a factor of 10 between each data set for clarity and the data points have been connected by a line to guide the eye. Data are shown for the azimuthal angular range between -35° and +35°. Obviously the quality of the coating in this angular range is uncompromised although a small degradation of the reflectivity curve is visible for the extreme cases of -35° and+35 °. The only significant variation is the change in the graze angle where the reflectivity drops due to the magnitude of the minimum bilayer thickness in the multilayer stack. This variation corresponds to a decrease of $d_{\rm min}$(and thus all bilayer thicknesses in the stack) as ϕ is going away from 0 on either side. To quantify this we have deduced $d_{\rm min}$ for each ϕ value for the 34 keV data by modeling the data as described in the next section. The $d_{\rm min}$-values are plotted in figure 4. An estimated uncertainty in this determination of $d_{\rm min}$ is indicated. The variation is small and the data indicate that up to ca. 30° on either side of 0 there is a near linear variation. As one goes above 30° on both sides the variation becomes increasingly steeper and the reflectivity begins to suffer. One further notes that the top point of the experimental curve does not coincide with thecentral spacer position where ϕ=0°. This is a trivial systematic shift due to the fact that the mirror segment was mounted during deposition with the symmetry point shifted ca. 5° away from what later became the central spacer position on the prototype. Conclusively one can see that the bilayer thickness changes ca. 5% in a 60° segment around the symmetry point. This is within the specification for the 60° segments of HEFT. We are, however, in the process of improving this result even further. Coating geomtries have recently been described for this type of cylindrical mirror segments which can reduce this variation to the 1% level.[19]

4. MODELING OF THE REFLECTIVITY DATA

A systematic prestudy and calibration of the deposition has been conducted which enabled the coating of the mirror segments with multilayers having a graded bilayer structure as prescribed in Table 1[16] . Based on this we have chosen to model the reflectivity data from the mirror segments using the nominal values of c and Γ as listed in Table 1. Obviously the number of bilayers is controlled and is a known parameter. We did, however, allow ourselves to vary the minimum bilayer thickness $d_{\rm min}$, the maximum bilayer thickness $d_{\rm max}$, and a small systematic misalignment of the graze angle on the order of 0.2 milliradian or less. We chose to constrain the interfacial width σ, to be the same throughout the multilayer stack for all the data sets. . $d_{\rm min}$ is well constrained for each data set as described in the last section but $d_{\rm max}$ is, however, less constrained by the data. We therefore tied the values of $d_{\rm max}$ to $d_{\rm min}$ in the sense that if $d_{\rm min}$ deviates from the nominal value of Table 1 we let $d_{\rm max}$ deviate the same percentage. We found that varying $d_{\rm max}$, independently, within reasonable limits, did not significantly improve the overall correspondance between the level of the reflectivity data and the model. The model calculations are performed using an X-ray reflectivity code for multilayered structures written by P.H.Mao.[8] The optical constants are obtained from the websites by L.Kissel and P.M.Bergstrom,Jr. at Lawrence Livermore National Laboratories(http://www-phys.llnl.gov/V_div/scattering/asf.html) and by J.H.Hubbell and S.M.Seltzer at the National Institute of Standards and Technology(http://physics.nist.gov/PhysRefData/XrayMassCoeff/cover/html).

4.1. Data and model for small ϕ values

Figure 5 shows the reflectivity data for all five mirror segments at 34 keV and ϕ= + 5° and our model calculations. Figure 6 shows the reflectivity data for mirror segments D1 through D4 at 65 keV and ϕ = -8° and the resulting model calculations and figure 7 shows the data and model for mirror segment D3 at 170 keV and ϕ=-8° and mirror

segment D4 at 158 keV and ϕ=-8°. At these small ϕ-values $d_{\min}$ should come very close to the nominal values of Table 1 and for the same mirror segment the model should predict very nearly the same $d_{\min}$ at the different energies. This is indeed the case as one can see from Table 2 which gives the value of $d_{\min}$ used in our model calculations in figures 5, 6, and 7. We estimate that the uncertainty in the determination of $d_{\min}$ from the data is 0.25 Å from residual alignment errors. This is less than 1%. The small discrepancy between the $d_{\min}$ values obtained at the different energies for the same mirror segment is consistent with this uncertainty. In addition a change of $d_{\min}$ is expected when going from ϕ=-8° to ϕ=+5° as demonstrated in Figure 4. From Figure 4 this variation may be on the order of 0.2 Å.

We found that a value of σ of 4.5 Å is consistent with the majority of our small ϕ-value data and this is used in the model calculations of figure 5, 6 and 7. The feature of the reflectivity data which constrains σ the most is the level of the reflectivity after the sharp drop in the reflectivity due to the magnitude of $d_{\min}$. The level of this reflectivity is due to the second order reflections in the graded d-spacing stack and to the extent the c and Γ value used in the modelling is correct this level of the second order reflectivies determines the value of σ. Some small variation in how well this level is fit by a single value of σ for all the small ϕ value data is observed. This could point to small variations of σ of order 0.1-0.3 Å with mirror segment and/or energy. We have, however, not found any significant systematic variation and all the small ϕ-value data are consistent with a σ value of 4.5 Å. Considering the extent of the energy range for these data this is in good agreement with the 4.3 Å obtained previously from modelling reflectivity data taken at 8 keV(data from DSRI) and data taken at 28 keV(data from BM5 at ESRF) from coated free standing mirror segments.[14] This implies that the interfacial width is due to lengthscales shorter than those probed even at the high energies leading to an energy independence of the multilayer model parameters.

4.2. Data and model for High ϕ values

To confirm that we can model the reflectivity of data taken at values of ϕ up to 30° away from the central spacer position on both sides, using appropriately adjusted $d_{\min}$ values as shown in figure 4, we show in figure 8 the reflectivity data and the model calculations for mirror segment D3 at the ϕ values -30°,-17°, +17° and +30°. We found that a value of σ of 4.5 Å fits the ϕ=-17° and ϕ=+17° data well but a slight increase of σ to 5.0 Å was required for the ϕ=-30 ° and the ϕ=+30° data. The values of $d_{\min}$ are the ones plotted in figure 4 for the respective ϕ-values.

5. IMAGING MEASUREMENTS

5.1. Experimental detail

The X-ray characterization of the imaging performance was performed at DSRI at 8 keV and at the ESRF at energies up to 170 keV. At the DSRI facility 8 keV X-rays from a rotating anode source are directed through a Ge(111) crystal monochromator and a set of slits to produce a low divergence monochromatic X-ray beam.[20] For these measurements a slit width of 0.3 mm was used providing an angular resolution of 35 arcsec FWHM. The beam footprint is ca. 2 mm in the azimuthal direction. The reflected and scattered X-rays are detected with a one dimensional position sensitive proportional counter located a distance of 2.3 m from the optic. The optic is held in a fixture that allows for remotely controlled translation and rotation during testing. After initial alignment the optic is rotated about an axis perpendicular to the optical axis to an incident angle(typically 0.15°) where the X-ray pencil beam illuminates the majority of the optic. Final alignment consists of translating the optic so that the beam footprint is centered for a nominal position on the mirror segment under study. The angular distribution of the reflected X-rays is then recorded and after each mirror segment is measured the optic is rotated in azimuth angle by 2° and the measurement is repeated. This test set up samples over 50% of the optical surface. At BM5 at ESRF we selected a 28 keV beam as described under the reflectivity measurements. In addition we selected a 68 keV beam using the Si(333) reflection together with an absorber to eliminate the Si(111)-reflection. At ID15 we selected a 170 keV beam for the imaging data. A CCD camera, optically coupled to an X-ray scintillator array provides two dimensional imaging at both beamlines. The camera was located at a distance of 2.6 m from the optic and provided an angular resolution of 35 arcsec FWHM.

5.2. Imaging data and results

During assembly of the prototype optics, mechanical metrology(e.g. the tolerances on the spacer machining as well as the conformance of the glass to the spacers) is used to monitor performance of the assembly procedure. This

metrology was used as input to a raytrace which predicted ca. 35 arcsecond angular resolution FWHM for the assembled one bounce optic.

X-ray imaging data was taken at 8 keV, 28 keV and 68 keV as well as a limited set of exposures at 170 keV. A histogram showing the distribution of individual pencil beam measurements for all mirror segments at 28 keV is presented in figure 9. The angular resolution of the probe beam is responsible for the cut off at ca 10 arcsecond. A substantial fraction of the individual pencil beam measurements are resolution limited. The data from these individual measurements, including intensity and detailed X-ray spatial profile, can be added to produce a radially averaged point spread function. For segmented optics, this approach best represents the performance of the final optics. Systematic errors in the alignment and in the fixture that rotates the optic shift the position of the X-ray spot and require that the raw data be corrected before the individual pencil beam measurements are combined. After this correction, and deconvolving by the probe beam, the data are combined to produce the radially averaged point spread function. Errors in the HPD determination, including statistical and residual systematics, are estimated to be +/- 2 arcseconds. The combined data for 28 keV are shown in figure 10.

The deduced HPD from data at 8, 28 and 68 keV are presented in Table 3. Nearly identical values, close to 35 arcsecond, are obtained at all energies and for all mirror segments included in the test(D2-D5). At 170 keV only a portion of the optics was sampled, however profiles are consistent with 35 arcsecond HPD. The HPD for a two bounce optics can be determined, for uncorrelated errors, by multiplying the one bounce number by $2^{1/2}$(See Jimenez-Garate et al[21] for a discusion of the error terms).

6. CONCLUSION

We have measured the X-ray reflectivity from 18 keV to 170 keV using synchrotron radiation from realistically sized W/Si multilayer coated mirror segments mounted in a single reflection cylindrical prototype for the hard X-ray telescopes which is to be flown on the High Energy Focusing Telescope balloon borne mission. It has been demonstrated that all the data can be well described by the intended power law distribution of the bilayer thicknesses which has been designed and optimized for the telescope performance and we have found that all the data are consistent with an interfacial width of 4.5 Å. A systematic and expected variation of the thickness uniformity of the coatings have been quantified and found to be ca. 5% over the foreseen area of the HEFT mirrors. This is well within the specifications. These results have enabled us to reliably predict the effective area and Field of View of both HEFT and the Hard X-ray Telecope on Constellation-X demonstrating that the specifications set for both of these missions are comfortably met based on measured reflectivities as presented in this paper.[22] We have also demonstrated that it is feasible to use similar W/Si multilayer coatings for much higher energies than the nominal energy range of HEFT. This leads the way for designing Gamma-ray telescopes for future astronomical applications as well as specialized applications of synchrotron radiation for the study of bulk properties of materials. Finally we have studied the imaging properties at 8, 28 and 68 keV of the one bounce prototype optics and have shown that we get nearly identical HPD in the entire energy band with a value close to 35 arcseconds. This value is consistent with the value predicted from mechanical metrology of the spacer machining. These results indicate that, at the level of 35 arcseconds, there is no energy dependent scattering contribution to the HPD. The HPD imaging goal for HEFT is 1 arcmin and the projected imaging performance as determined from the results presented in this paper is well below this specification.

7. ACKNOWLEDGMENTS

We are grateful R. Hustache of the ESRF for expert technical assistance during the measurements.

REFERENCES

1. F.E.Christensen, A.Hornstrup, N.J.Westergaard, H.W.Schnopper, J.L.Wood, and K.Parker, "A graded d-spacing multilayer telescope for high energy x-ray astronomy," *Proc. SPIE* **1546**, pp. 160–167, 1992.
2. K.D.Joensen, F.E.Christensen, H.W.Schnopper, P.Gorenstein, J.Susini, P.Hoghoj, R.Hustache, J.L.Wood, and K.Parker, "Medium-sized grazing incidence high-energy x-ray telescopes employing continuously graded multilayers," *Proc. SPIE* **1736**, pp. 239–248, 1993.
3. K.D.Joensen, P.Voutov, A.Szentgyorgyi, J.Roll, P.Gorenstein, P.Hoghoj, and F.E.Christensen, "Design of grazing-incidence multilayer supermirrors for hard x-ray reflectors," *Applied Optics* **34**, pp. 7935–7944, 1995.

4. F.A.Harrison, S.Boggs, A.Bolotnikov, W.Cook, P.H.Mao, S.Schindler, C.J.Hailey, W.W.Craig, M. Jimenez-Garate, D.L.Windt, F.E.Christensen, and C.P.Jensen, "Development of the balloon-borne high energy focusing telescope mission(heft)," *Proc. SPIE* **4012**, 2000.
5. K. Yamashita, P. Serlemitsos, J. Tueller, S. Barthelmy, L. Bartlett, K. Chan, A. Furuzawa, N. Gehrels, K. Haga, H. Kunieda, P. Kurczynski, G. Lodha, N. Nakajo, N. Nakamura, Y. Namba, Y. Ogasaka, T. Okajima, D. Palmer, A. Patsons, Y. Soong, S. Stahl, H. Takata, K. T. Y. Tawara, and B. Teegarden, "Supermirror hard x-ray telescope," *Applied Optics* **37**, pp. 8067–8073, 1998.
6. *Proc. of the High Throughput X-ray Spectroscopy Workshop* , 1996.
7. F.A.Harrison, W.Cook, F.E.Christensen, O. Citterio, W.W.Craig, N. Gehrels, P. Gorenstein, J. Grindlay, C.J.Hailey, R. Kroeger, H. Kunieda, A. Parsons, R. Petre, S. Romaine, B. Ramsey, J. Tueller, M. Ulmer, M. Weisskopf, and D.L.Windt, "Technology development for the constellation-x hard x-ray telescope," *Proc. SPIE* **3765**, 2000.
8. P.H.Mao, F.A.Harrison, D.L.Windt, and F.E.Christensen, "Optimization of graded multilayer designs for astronomical x-ray telescopes," *Applied Optics* **38**, pp. 4766–4775, 1999.
9. D.L.Windt, F.E.Christensen, W.W.Craig, C.J.Hailey, F.A.Harrison, M.A.Jimenez-Garate, and P.H.Mao, "X-ray multilayers for use at energies above 100 kev," *Proc. SPIE* **4012**, 2000.
10. K. Yamashita, H. Kunieda, Y. Tawara, K. Tamura, Y. Ogasaka, K. Haga, T. Okajima, Y. Hidaka, S. Ichimaru, S. Takahashi, A. Goto, H. Kito, Y.Tsusaka, K. Yokoyama, and S. Takeda, "New design concept of multilayer supermirrors for hard x-ray optics," *Proc. SPIE* **3766**, pp. 327–335, 1999.
11. C.J.Hailey, S.Abdali, F.E.Christensen, W.W.Craig, T.R.Decker, F.A.Harrison, and M.A.Jimenez-Garate, "Substrates and mounting techniques for the high energy focusing telescope," *Proc. SPIE* **3114**, pp. 535–543, 1997.
12. W.W.Craig, F.E.Christensen, T.R.Decker, C.J.Hailey, F.A.Harrison, R.Hill, M.A.Jimenez-Garate, P.H.Mao, and S.Schindler, "Hard x-ray optics for the heft balloon-borne payload: prototype design and status," *Proc. SPIE* **3445**, pp. 112–120, 1998.
13. W.W.Craig, F.E.Christensen, C.J.Hailey, F.A.Harrison, A.M.Hussain, M.A.Jimenez-Garate, P.H.Mao, and D.L.Windt, "Hard X-ray Imaging Performance of Thermally Formed Glass Optics," *Science* , submitted.
14. A.M.Hussain, F.E.Christensen, M.A.Jimenez-Garate, W.W.Craig, C.J.Hailey, T.R.Decker, M.Stern, D.L.Windt, P.H.Mao, F.A.Harrison, G.Pareschi, M.D. Rio Sanchez, A.Souvorov, A.K.Freund, R.Tucoulou, A.Madsen, and C.Mammen, "X-ray scatter measurments from thermally slumped thin glass substrates for the heft hard x-ray telescopes," *Proc. SPIE* **3766**, pp. 184–196, 1999.
15. D.L.Windt and W.K.Waskiewicz *J. Vac. Science Technology* **B12**, pp. 3826–3832, 1994.
16. D.L.Windt, F.E.Christensen, W.W.Craig, C.J.Hailey, F.A.Harrison, M.A.Jimenez-Garate, R. Kalyanaraman, and P.H.Mao, "Growth, structure and performance of depth-graded w/si multilayers for hard x-ray optics," *J. Appl. Physics* , submitted.
17. F.E.Christensen, F.A.Harrison, S. Boggs, P.H.Mao, W.W.Craig, C.J.Hailey, and T. Prince, "Grazing incidence optics for future gamma ray missions," *Proc. SPIE* **4012**, 2000.
18. P.H.Mao, F.A.Harrison, Y.Y.Platonov, D.Broadway, B.DGroot, F.E.Christensen, W.W.Craig, and C.J.Hailey, "Development of grazing incidence multilayer mirrors for hard x-ray focusing telescopes," *Proc. SPIE* **3114**, pp. 526–534, 1997.
19. D. Broadway, Y. Platonov, and L. Gomez, "Achieving desired thickness gradients on flat and curved substrates," *Proc. SPIE* **3766**, pp. 262–274, 1999.
20. F.E.Christensen, S.Abdali, A.Hornstrup, H.W.Schnopper, P.Slane, and S.E.Romaine, "High resolution x-ray scatter and reflectivity study of sputtered ir surfaces," *Proc. SPIE* **2011**, pp. 18–33, 1994.
21. M.A.Jimenez-Garate, W.W.Craig, and C.J.Hailey *Proc. SPIE* **3444**, 1998.
22. F.E.Christensen, W.W.Craig, J.M.Chakan, C.J.Hailey, F.A.Harrison, V.Honkimaki, M.A.Jimenez-Garate, P.H.Mao, D.L.Windt, E.Ziegler, "Measured Reflectance of Graded Multilayer Mirrors Designed for Astronomical Hard X-ray Telescopes," *Nuclear Instruments and Missions A*, submitted.

Table 1. *HEFT* multilayer design.

Mirror group	Angular range [mrad]	Radial range [cm]	$d_{\min}$ [Å]	$d_{\max}$ [Å]	c	Γ	N	Coating thickness [μm]
D1	1.67-1.86	4.00-4.46	33.3	297.6	0.225	0.40	150	0.66
D2	1.86-2.08	4.46-4.99	29.9	266.6	0.230	0.40	200	0.79
D3	2.08-2.32	4.99-5.57	28.7	238.9	0.220	0.40	250	0.93
D4	2.32-2.59	5.57-6.22	27.4	214.0	0.225	0.40	250	0.90
D5	2.59-2.89	6.22-6.94	26.1	191.8	0.220	0.40	300	1.01
D6	2.89-3.22	6.94-7.73	24.7	171.8	0.215	0.40	350	1.11
D7	3.22-3.60	7.73-8.64	24.6	153.9	0.200	0.40	350	1.08
D8	3.60-4.01	8.64-9.62	24.3	137.9	0.205	0.35	350	1.08
D9	4.01-4.48	9.62-10.75	23.7	123.6	0.200	0.35	350	1.04
D10	4.48-5.00	10.75-12.0	23.0	110.7	0.195	0.35	350	1.00

Table 2. Modelled minimum d-spacings.

Mirror segment	ϕ deg	Energy keV	$d_{\min}$ [Å]
D1	+5	34	34.6
D1	-8	65	34.3
D2	+5	34	30.8
D2	-8	65	30.2
D3	+5	34	29.4
D3	-8	65	29.6
D3	-8	170	29.6
D4	+5	34	27.6
D4	-8	65	27.5
D4	-8	158	28.0
D5	+5	34	26.4

Table 3. The HPD of the individual mirror segments in arcseconds.

Mirror segment	8 keV	28 keV	68 keV
D2	31	29	-
D3	35	36	33
D4	33	31	-
D5	33	34	-

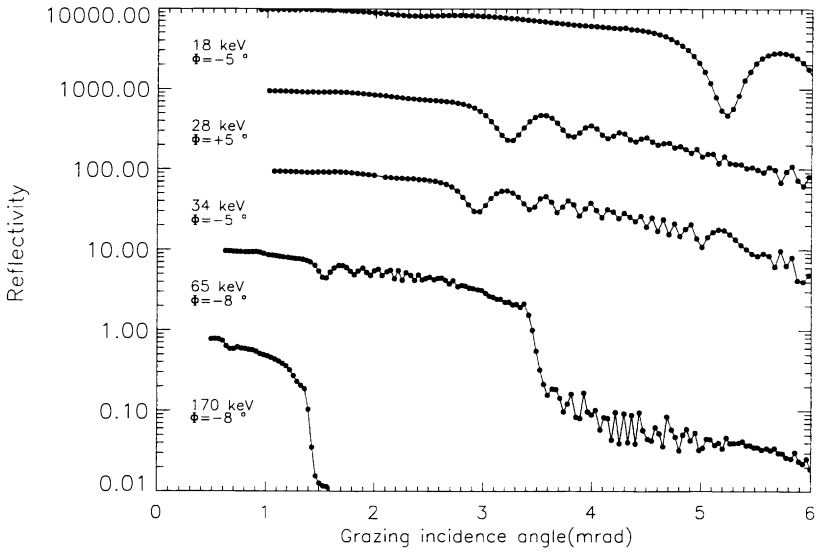

Figure 1. Measured reflectivity of mirror segment D3 at energies from 18 keV to 170 keV. The line between data points is a guide for the eye. Data sets has been shifted by a factor of 10 for clarity. The ϕ-values at which the data are taken are indicated.

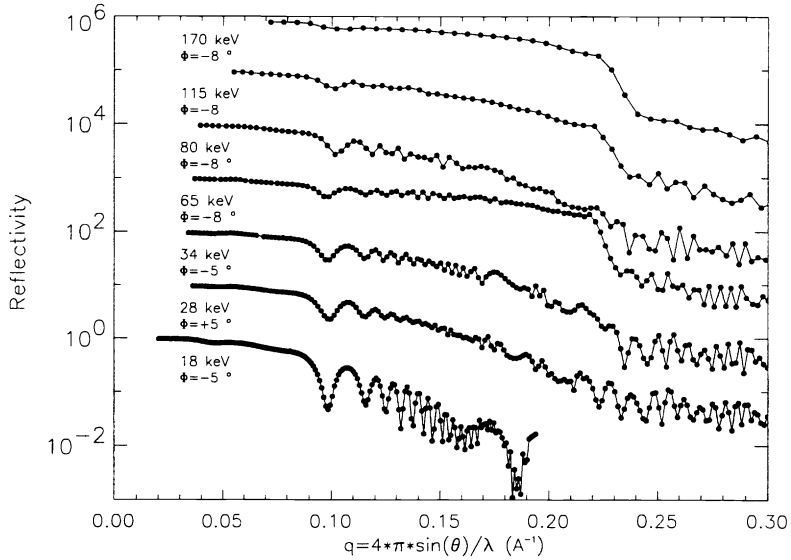

Figure 2. Reflectivity data from mirror segment D3 plotted versus reciprocal lattice vector q. The line between data points is a guide for the eye. The data sets are shifted a factor of 10 for clarity and the energy and ϕ-value for each data set is indicated. The effect of the K-absorption edge of W is clearly visible in the 80 keV data. At 170 keV the reflectivity has completely recovered and high reflectivity is measured out to ca. 3 times the critical angle.

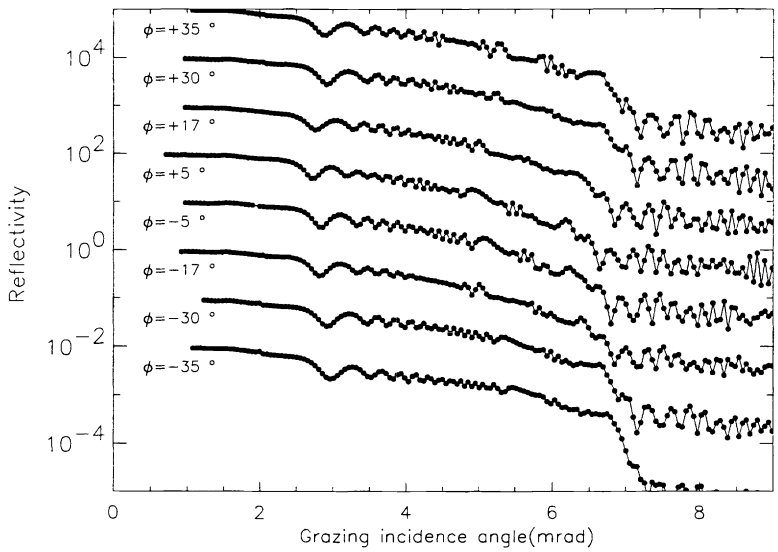

Figure 3. The measured reflectivity for different ϕ-values ranging from -35° to +35°. The data are from mirror segment D3 and taken at 34 keV. The data points are connected by a line as a guide for the eye and the data sets are shifted by a factor of 10 for clarity.

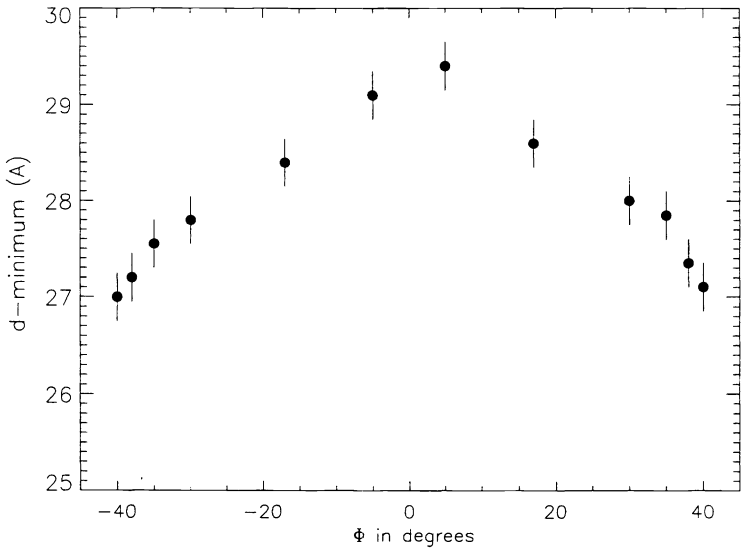

Figure 4. Deduced minimum bilayer thicknesses versus ϕ from 34 keV data from mirror segment D3. The variation is small and is near 5% in a 60° segment around the symmetry top point.

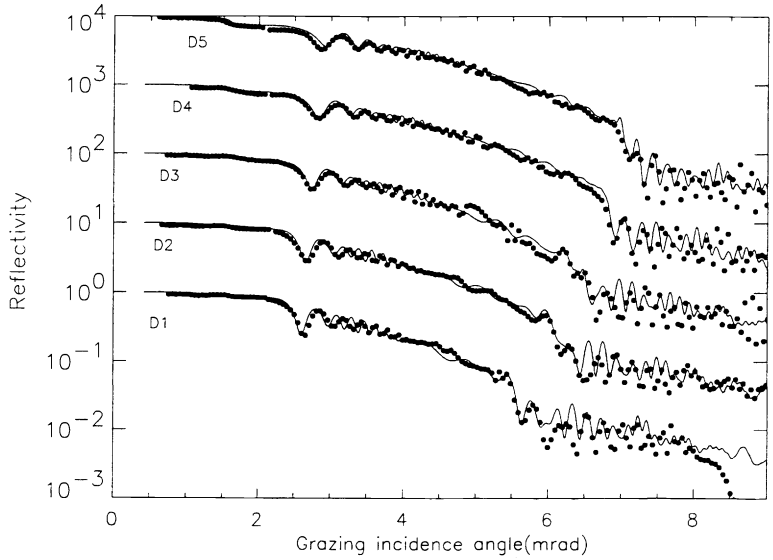

Figure 5. Data and model as described in the text for all mirror segments at 34 keV and ϕ=+5°. The full line is the model calculation.

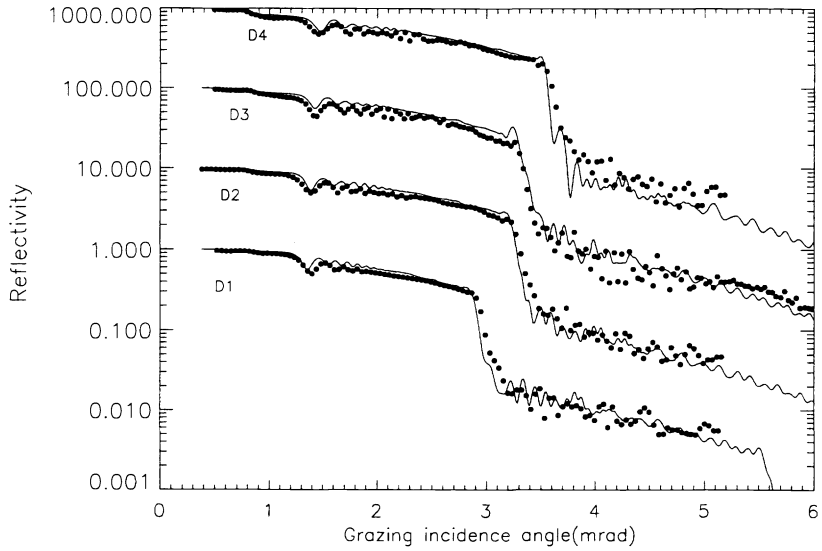

Figure 6. Data and model as described in the text for mirror segments D1,D2,D3 and D4 at 65 keV and ϕ=-8°. The full line is the model calculation.

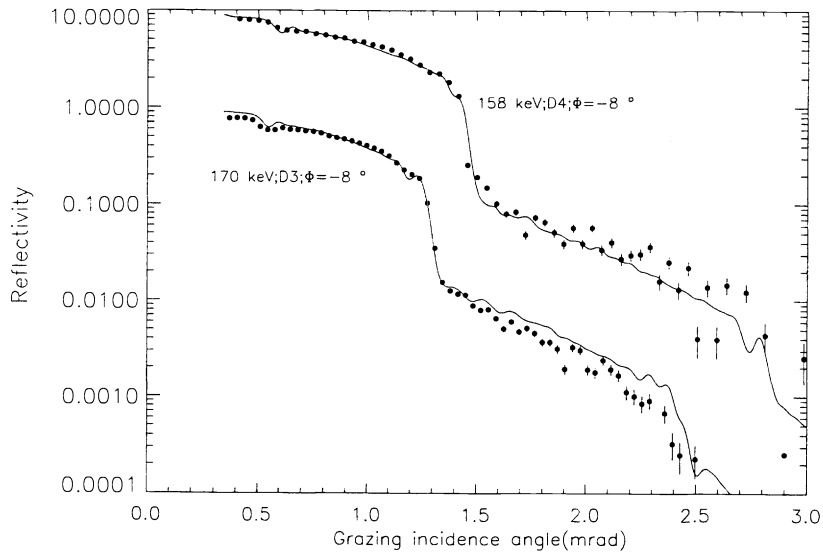

Figure 7. Data and model as described in the text for mirror segment D3 at 170 keV and ϕ=-8° and mirror segment D4 at 158 keV and ϕ=-8°. The full line is the model calculation.

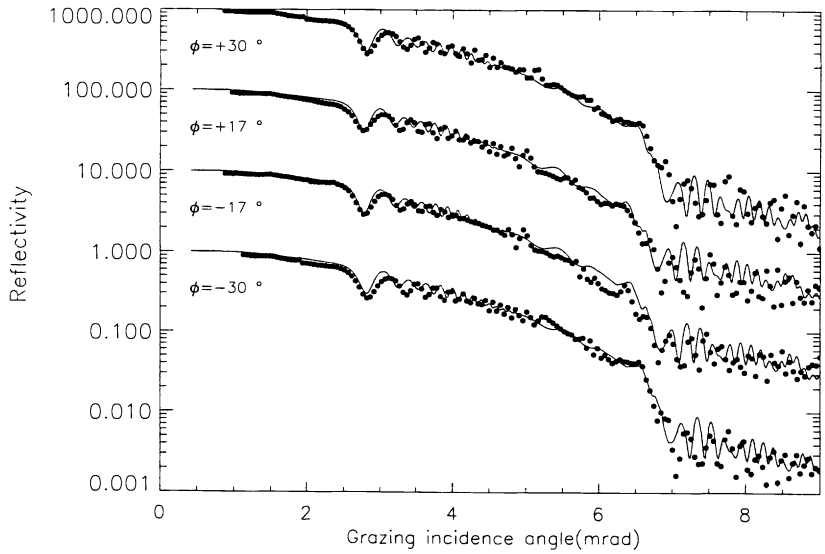

Figure 8. Data and model as described in the text for mirror segment D3 at 34 keV and ϕ-values -30° ,-17° ,+17° ,+30°. The full line is the model calculation.

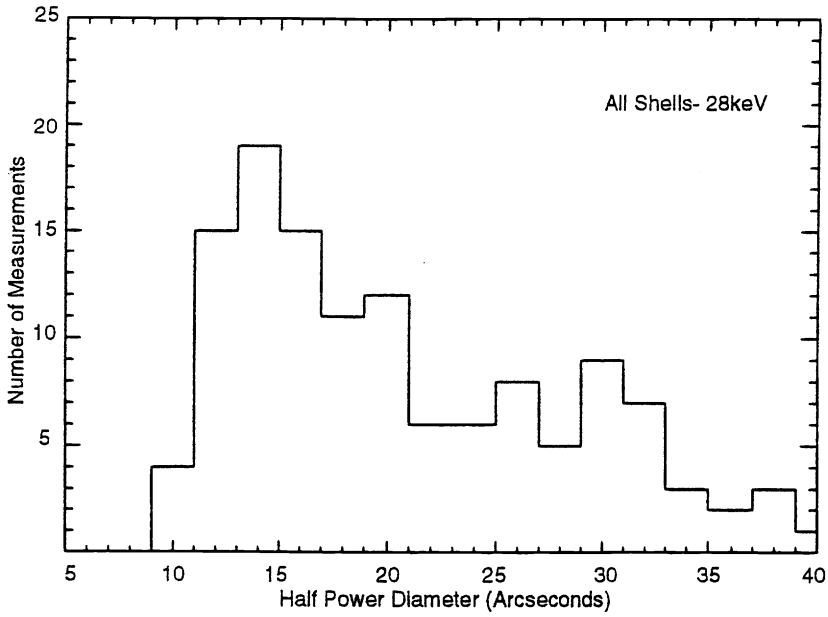

Figure 9. Distribution of HPD measurements for all mirror segments at 28 keV.

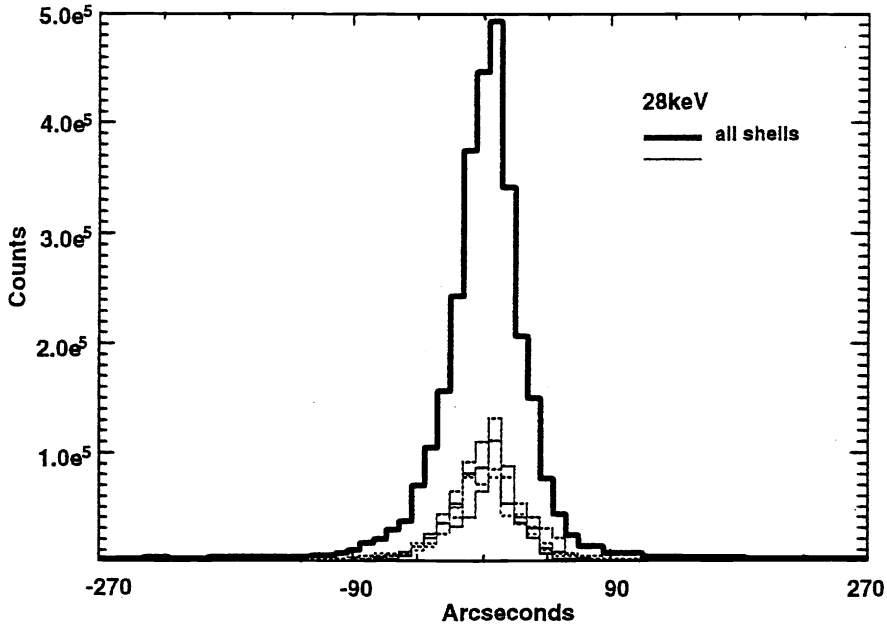

Figure 10. The radially averaged Point Spread Function for all the mirror segments in the prototype. The heavy solid line is the sum. The individual mirror segment contributions are also shown.